Inorganic Chemistry

Article

pubs.acs.org/IC

Discovery of γ-MnP_4 and the Polymorphism of Manganese Tetraphosphide

Dennis B. Henge,[†,∥] Martin Hermus,[‡,∥] Christian F. Litterscheid,[†] Norbert Wagner,[§] Johannes Beck,[§] Barbara Albert,*[,†] and Jakoah Brgoch*[,‡]

[†]Eduard-Zintl-Institute of Inorganic and Physical Chemistry, Technische Universität Darmstadt, Alarich-Weiss-Str. 12, 64287 Darmstadt, Germany

[‡]Department of Chemistry, University of Houston, Houston, Texas 77204, United States

[§]Institute of Inorganic Chemistry, Rheinische Friedrich-Wilhelms-Universität Bonn, Gerhard-Domagk-Str. 1, 53121 Bonn, Germany

Supporting Information

ABSTRACT: A new polymorph of MnP_4 was prepared by reaction of the elements via chemical vapor transport with iodine as transporting agent. The crystal structure was refined using single-crystal diffraction data (space group *Cc*, no. 9, a = 5.1049(8) Å, b = 10.540(2) Å, c = 10.875(2) Å, β = 93.80(2)°). The phase is called γ-MnP_4 as it is isostructural with γ-FeP_4. It is the fourth reported binary polymorph in the MnP_4 system, all of which are stacking variants of nets built with manganese and phosphorus atoms. In γ-MnP_4, there are two Mn−Mn distances (2.93 and 3.72 Å) arising from a Peierls-like distortion effectively forming Mn_2 dumbbells in the structure. Magnetic and electrical conductivity measurements show diamagnetism and a small anisotropic band gap (100−200 meV) with significantly enhanced conductivity along the crystallographic a axis. Calculations of the electronic and vibrational (phonon) structures show the P−P and Mn−P bonds within the nets are mainly responsible for the stability of the phase. The similar bonding motifs of the polymorphs give rise to the existence of numerous dynamically stable variants. The calculated Helmholtz energy shows the polymorph formation to be closely tied to temperature with the 6-MnP_4 structure favorable at low temperatures, the 2-MnP_4 favorable between approximately 800 and 2000 K, and 8-MnP_4 preferred at high temperatures.

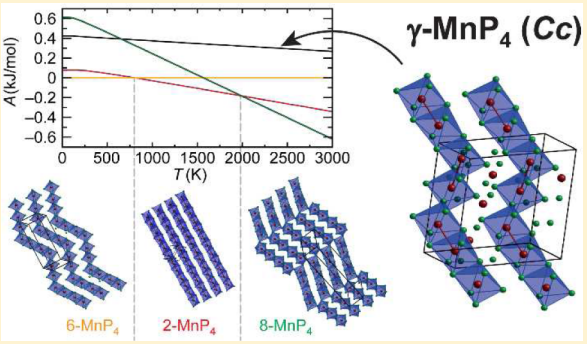

INTRODUCTION

The ability of phosphorus to exist as isolated anion as well as in a network of polyanions with covalent P−P bonds leads to a large variety of metal phosphides in different stoichiometries ranging from metal-rich phosphides, like M_3P (M = Cr, Mn, Fe, Co, Ni, Cu) to polyphosphides such as the reported MnP_4.[1,2] Due to the abundance of compositions and structures, strongly varying physical properties are observed ranging from metallic behavior in the metal-rich phosphides with magnetic ordering, to diamagnetic semiconducting or insulating compounds in the phosphor-rich realm. For instance, superconductivity is observed in transition-metal-rich phosphors like MoRuP and MoNiP, which show transition temperatures above 15 K, the highest values for metal phosphides.[3] Even fascinating properties are observed in the binary MnP phase by showing pressure induced superconductivity.[4] On the phosphorus-rich side, metal polyphosphides have been used as anode material for Li-ion batteries.[5] Promising results have shown the successful insertion of Li into MnP_4 to reversibly form Li_7MnP_4 by cleaving (reduction) of the P−P bonds.[6] Unfortunately, the parent MnP_4 crystal structure forms multiple polymorphs and it is unclear how to control the crystallization process necessary to advance this technology.

Initially, three polymorphs of the binary MnP_4 were identified that contain modified stacking patters of the Mn_2P_4 hexagonal units.[7−9] In these three structures, the hexagons stack in repeating units of 2, 6, or 8 times in one translational period. Thus, they are named according to the stacking of layers of pentagons and hexagons formed by manganese and phosphorus: 2-MnP_4,[8] 6-MnP_4,[9] and 8-MnP_4.[7] A second description of the polymorphism in this compound is based on the corner- or edge-sharing TP_6 octahedra (T = transition metal), which is used to describe the crystal structure of γ-FeP_4.[10,11] This description is visualized in Figure 1, with the octahedral units highlighted in blue. The stacking variants in this description modify the lengths of the linear octahedral chains. For example, 2-MnP_4 contains infinite linear chains of edge sharing MnP_6 octahedra. In 6-MnP_4, a change of direction in the chains is observed after four units, so that a zigzag-chain emerges. A zigzag-chain is also observed in 8-MnP_4 with linear

Received: June 22, 2015
Published: August 12, 2015

DOI: 10.1021/acs.inorgchem.5b01372
Inorg. Chem. 2015, 54, 8761−8768

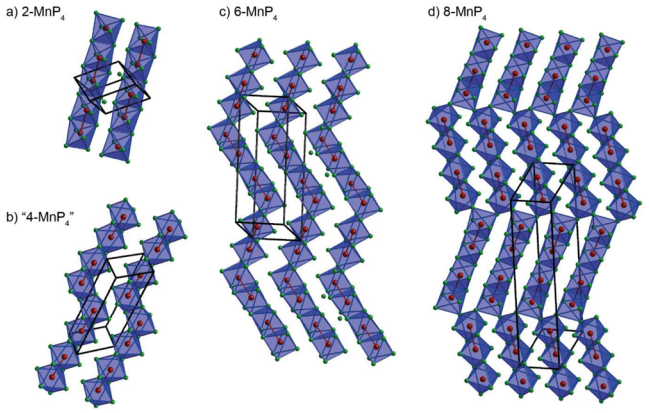

Figure 1. Crystal structures of the four known modifications of MnP_4. Mn is shown in red, P is shown in green, and the MnP_6 octahedra are highlighted in blue.

segments of four edge-sharing octahedra connected via corners. A fourth polymorph in the series was discovered from the synthesis of a solid solution with transition metals Mn and Cr, $Mn_{1-x}Cr_xP_4$ ($0.3 < x < 0.7$). Although a pseudobinary composition, the similarity of this stacking variant led to it being named "4-MnP_4."[12] The incorporation of Cr in this solid solution is an example of the many more transition metal tetraphosphides TP_4, which are known: the CrP_4-type (space group $C2/c$, T = Cr, Mo, V),[13] α-OsP_4 type ($P2_1/c$, T = Ru, Os, Mg, Cd),[14] or the other FeP_4-variants (see refs 10,11 and references therein). There exist further modifications of TP_4 with different space groups (T = Ru, Os: $P\bar{1}$:,[15] T = Re, Tc: $Pbca$,[16,17] and ZnP_4: $P4_12_12$)[18,19] In nearly all of these compounds, layers of transition metal atoms and phosphorus atoms form the crystal structure.

Such similar crystal chemistry among these compounds makes it extremely difficult to synthesize these as phase pure samples. Often more than one polymorph is present in the product. For example, 8-MnP_4 was initially synthesized under extreme conditions (e.g., 30 kbar to 55 kbar and 1500 to 1700 K). Even with these difficult synthetic conditions, unidentified phases remained present in the product.[7] Using a Sn-flux, 8-MnP_4 and ultimately two other polymorphs 2-MnP_4[8] and 6-MnP_4[9] were identified with reaction temperatures ranging between 820 and 1200 K. The stacking variant "4-MnP_4", formed by $Mn_{1-x}Cr_xP_4$ ($0.3 < x < 0.7$), was also obtained from a Sn-flux at high temperature (948 K).[12] Only one single-phase product of 2-MnP_4 has been obtained so far.[9] In this case, iodine transport in a temperature gradient produced the desired crystal structure as a single phase at the cool end of a tube while the hot end of the tube contained the alternate polymorphs.

It is clear that polymorph control is very difficult to achieve in this system. Therefore, the work presented here examines the electronic structure and thermodynamics of the phase space of MnP_4 to provide insight that will aid synthetic control over polymorphs formation. During our synthetic work on manganese polyphosphides using chemical vapor transport with iodine as transporting agent, a new binary MnP_4 polymorph was obtained. This new structural variant represents the previously "missing" binary 4-MnP_4 structure, as solved by single-crystal X-ray diffraction. The identification of this new phase further supports the current lack of synthetic control over structure formation. Using first-principles calculations, the electronic structure and vibrational properties are reported for all of the polymorphs to address the origin of phase formation. From our results, we suggest a path to synthetically target a given MnP_4 polymorph in this complex crystal system.

EXPERIMENTAL SECTION

Synthesis. Starting materials including manganese powder (Sigma-Aldrich, 99.99%) and red phosphorus (Preussag, > 99.99%) were mixed with a molar ratio of Mn:P of 1:4. Small amounts of iodine as transporting agent were added. The samples were sealed in evacuated silica tubes and annealed in a temperature gradient of 1073 to 923 K for 2 weeks. The new modification crystallized at the cold end of the ampule, together with other Mn−P phases. Attempts to make a phase pure sample of this new crystal structure led to a mixture of all polymorphs regardless of reaction conditions, highlighting the difficulty of synthesizing these phases as bulk powders.

Sample Characterization. Scanning electron microscopy and energy-dispersive X-ray spectroscopy were performed on a Jeol JSM-6400 instrument with an APOLLO X Silicon Drift detector. Several crystals were analyzed. X-ray powder patterns were collected on a transmission powder diffractometer (Stoe Stadi P, Darmstadt, Germany) using germanium-monochromatized Mo Kα1 radiation (λ = 0.70932 Å) with a flat plate sample holder and a linear position sensitive detector. Data for single-crystal determination was obtained using a diffractometer (Stoe IPDS2, Darmstadt, Germany) with Mo Kα radiation (λ = 0.71073 Å). Structure refinement was performed using the program SHELX.[20] Magnetic measurements were performed with a Quantum Design PPMS in a temperature range of 2 to 300 K with a magnetic field of 10000 Oe. Measurements of electrical resistivity were done on single-crystals in the range of 280 to 330 K with a two- and a four-probe technique, measuring different directions of the crystal (Figure S4).

DFT Calculations. The electronic structures of the experimentally phases have been calculated by means of density functional theory. The mixed occupancies in the pseudobinary "4-MnP_4" crystal structure were treated with the sites fully occupied by Mn. The Vienna Ab initio Simulation Package (VASP)[21,22] was used to determine the lowest energy structures. Plane-wave basis sets and projector-augmented-wave (PAW) potentials were used.[23] Correlation and exchange have been treated with the generalized gradient approximation (GGA) in the parametrization of Perdew, Burke, and Ernzerhof.[24] A cutoff energy of 500 eV was chosen and a dense Gamma-centered Monkhorst−Pack k-point grid (at least 1000 k-points/atoms^{-1})[25] was used for integrations within the Brillouin zone. Forces, stress tensors, atomic positions, unit cell shapes, and unit cell volumes were allowed to relax. The convergence criterion of the structural electronic structure calculation was set to 1×10^{-6} eV for the ionic relaxation and 1×10^{-8} eV for the electronic relaxation. On the electronically and structurally relaxed structures, first-principles scalar-relativistic electronic structure calculations and chemical bonding analyses were performed by means of the linear muffin-tin orbital method (LMTO).[26,27] The LMTO calculations were carried out using the tight binding (TB) representation[28] within the atomic spheres approximation (ASA)[29] as implemented in the STUTTGART TB-LMTO-ASA 4.7 program.[30] The electronic energy was calculated using the local exchange correlation functional in the parametrization of Vosko, Wilk, and Nusair[31] with the nonlocal corrections of exchange and correlation by Perdew and Wang.[32] Brillouin zone integrations used an improved tetrahedron method.[33] Self-consistency was achieved when the total-energy change was smaller than 1×10^{-4} eV. Chemical bonding analyses were based on the density of states (DOS) and crystal orbital Hamilton populations (COHP).[34] The ICOHP values and the corresponding distances listed in Table 3 are tabulated as symmetry-weighted arithmetic averages. The vibrational properties were calculated with PHONOPY,[35] which is based on the ab initio force constant method.[36] To construct the force constant matrix forces were calculated by VASP on supercells, in which symmetry independent atoms are displaced from their equilibrium position by 0.01 Å. The Helmholtz energy was calculated as the sum of the electronic ground

DOI: 10.1021/acs.inorgchem.5b01372
Inorg. Chem. 2015, 54, 8761−8768

state energy and the vibrational contributions from the phonon frequencies.

RESULTS AND DISCUSSION

Crystal Structure. From the synthesis of MnP_4 using vapor transport, well-faceted single crystals were obtained with an arrowhead like morphology. They are twinned according to scanning electron microscopy (Figure 2a). Crystals of metallic

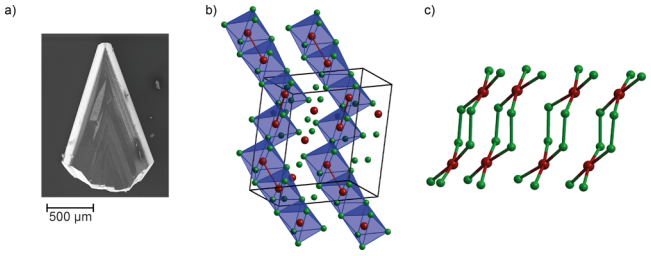

Figure 2. (a) Scanning electron micrograph of a crystal of γ-MnP_4 with the typical shape of twinning. (b) Unit cell of binary γ-MnP_4 with Mn is shown in red, P is shown in green, and the MnP_6 octahedra are highlighted in blue. (c) Four hexagons as repetition pattern for γ-MnP_4.

appearance were found to be air-stable as well as not visibly attacked by nonoxidizing acids. Energy dispersive X-ray spectroscopy of several crystals showed a ratio of 20 at. % to 80 at. % for manganese to phosphorus in accordance with the assumed composition.

The crystal structure was solved using several data sets collected for twinned crystals. Due to the severe twinning, it proved impossible to solve the crystal structure with direct methods based independently on the single-crystal diffraction data. Furthermore, the powder diffraction patterns collected on selected and crushed single crystals of the new phase indicated the pattern was different compared to the previously reported MnP_4 modifications.[7−9,12] Instead the collected pattern was similar to γ-FeP_4[11] crystallizing in Laue group $2/m$ with the monoclinic space group $C2/c$.

The structure analysis was first attempted using γ-FeP_4 in the centrosymmetric space group $C2/c$, with the asymmetric unit containing two Mn atoms on special positions, resulting in only a single Mn−Mn distance. This refinement produced implausible anisotropic atomic displacement parameters on the Mn sites (Table S3). Decreasing the symmetry to the noncentrosymmetric subgroup Cc allows the Mn atoms to displace and sit off-center in the octahedra. The resulting Flack x parameter of 0.31(3) is evidence of inversion twinning, which was taken into account by the TWIN option during refinement. The result is two independent Mn−Mn distances, 2.933(2) Å and 3.716(2) Å, in agreement with the other polymorphs.[7−9] The presence of two Mn−Mn bond lengths here is comparable to MnB_4, which also contains two Mn−Mn distances that arise from a Peierls-like distortion.[37,38] An analogous calculation of γ-MnP_4 in space group $C2/c$ with only one Mn−Mn distance indicates a large degeneracy in the density of states at the Fermi level that is not relieved through spin-polarization. This suggests a Peierls-like distortion is also the mechanism for Mn−Mn dimer formation in γ-MnP_4. Moreover, the structure calculated in $C2/c$ has a total energy that is ≈300 meV per formula unit higher than the structure in the correct space group, Cc. As a result, Cc is clearly the correct space group. The crystallographic and structural information for the refinement

Table 1. Data Collection and Crystallographic Parameters of γ-MnP_4

specimen	MnP_4
cryst syst	monoclinic
space group	Cc (No. 9)
a/Å	5.1049(8)
b/Å	10.5401(2)
c/Å	10.8751(2)
β/°	93.804(2)
V/Å^3	583.9(2)
Z	8
ρ_c/g/cm^3	4.069
F(000)	680
radiation	Mo Kα, λ = 0.71073 Å
reflns collected	5303
independent reflns	1525
reflns with $I > 2\sigma(I)$	1397
no. of params	93
θ-range/°	3.76−29.07
R (all data)	0.0303
wR_2 (all data)	0.0642
GOF	1.014
Flack x Parameter	0.31(3)

in Cc is given in Table 1 and Table 2 (and Table S1) with the crystal structure shown in Figure 2b. Data for the refinement in the wrong space group $C2/c$ is given in the Supporting Information (Table S2 and S3).

Table 2. Positional and Equivalent Displacement Parameters from the Single-Crystal Structure Refinement of γ-MnP_4[a]

atom	Wyck.	x/a	y/b	z/c	U_{eq}/ Å^2
Mn1	4a	0.2873(2)	0.27186(6)	0.52338(6)	0.0046(2)
Mn2	4a	0.0065(2)	0.10030(6)	0.24665(7)	0.0038(2)
P1A	4a	0.3109(3)	0.2537(2)	0.3047(2)	0.0056(3)
P1B	4a	0.7012(2)	0.2541(2)	0.2260(1)	0.0046(2)
P2A	4a	0.2166(2)	0.4443(2)	0.2240(1)	0.0048(2)
P2B	4a	0.8193(2)	0.4495(2)	0.28864(9)	0.0056(3)
P3A	4a	0.0828(2)	0.0716(2)	0.0488(1)	0.0057(3)
P3B	4a	0.9866(3)	0.1148(2)	0.4590(2)	0.0050(2)
P4A	4a	0.0931(2)	0.3804(2)	0.0341(2)	0.0054(2)
P4B	4a	0.9758(2)	0.4184(2)	0.4832(1)	0.0055(3)

[a] U_{eq} is defined as 1/3 of the trace of the orthogonalized U_{ij} tensor.

In this newly discovered phase, four layers form the repetition pattern, highlighted in Figure 2c. If the modification were named according to the stacking of layers of pentagons and hexagons formed by Mn and P atoms, this modification should be named 4-MnP_4. However, due to earlier assignment of the "4-MnP_4" to the pseudobinary $Mn_{1-x}Cr_xP_4$ solid solution, which also has a 4-unit translation period, we chose to name the new modification γ-MnP_4 as it is analogous to γ-FeP_4.[11] Following the Rühl−Jeitschko symbolism, which uses the conformation and sequence of the Mn_2P_4 units to describe the structure,[9] the new γ-MnP_4 phase is described as p′o′po, where o (ortho) and p (para) describe the position of the phosphorus atoms with two metal neighbors within the hexagons, while p and p′ (or o and o′, respectively) are mirror images of each other, with the mirror plane through the two

DOI: 10.1021/acs.inorgchem.5b01372
Inorg. Chem. 2015, 54, 8761−8768

manganese atoms and perpendicular to the layer. This MnP_4 modification shares great similarity to the previously identified polymorphs because of these pentagonal and hexagonal stacking sequences. Next-neighbor environments are also similar for the different modifications. Phosphorus atoms surround manganese atoms almost octahedrally with one face capped by another Mn atom. The Mn−P bonding lengths vary from 2.24 to 2.40 Å. Four atoms, either two other phosphorus atoms and two manganese atoms or three other manganese atoms and one other manganese atom, surround each phosphorus atom. Of these surrounding atoms, three are in the same layer as the central atom, while one is in the next layer. In the first case (P_2Mn_2 coordination), one of the manganese atoms is always in the next layer while in the second case (P_3Mn coordination) it is a phosphorus atom, which builds the bridge to the next layer. The nearest-neighbor interactions in MnP_4 were earlier described as covalent bonding.[8,9] Based on the octet rule this leads to a d^5 electron configuration for Mn and an oxidation number of +2 (see ref 12 and references cited therein).

Physical Properties. The magnetic susceptibilities of a sample consisting of selected single crystals are shown in Figure 3a. The new modification is diamagnetic, as it was expected

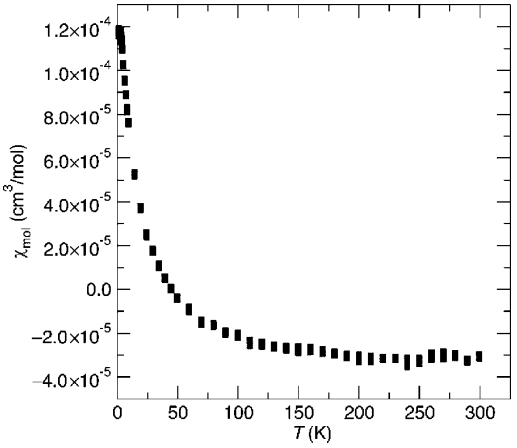

Figure 3. Temperature-dependent measurement of the magnetic susceptibility of γ-MnP_4.

from the electron configuration and as well as the magnetic properties of the other modifications of MnP_4.[8,9,12] Small amounts of paramagnetic impurities become visible at low temperatures.

For the exploration of the electric conductivity properties of γ-MnP_4 a large, needle-shaped crystal of length 1.8 mm was examined. The identity of the crystal was checked by X-ray diffraction, which gave the unit cell parameters corresponding to the γ phase. The face indexing of the crystal revealed the needle axis to be coincident with the crystallographic *a* axis. Two different measurement methods were applied: a four-probe measurement along the crystal axis and two probe measurements along and perpendicular to the needle axis. Photographic views of the examined crystal and of the different measurement setups are provided in the Supporting Information (Figures S1 to S4). In the temperature region between ambient temperature and 375 K the electrical resistivity decreases with temperature (Figure 4), similar to what has been observed for 6-MnP_4. A significant difference in the conductivity along and perpendicular to the crystal main axis is present.

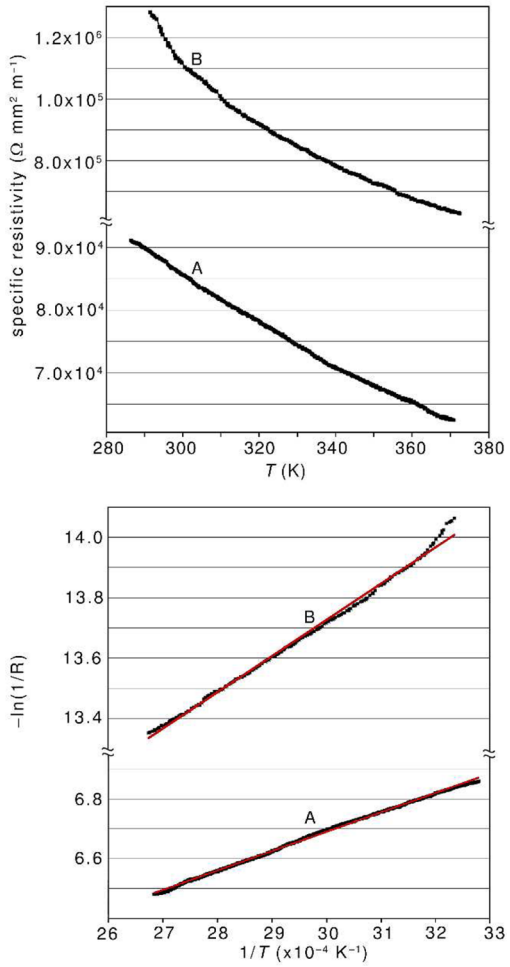

Figure 4. Electrical conductivity of γ-MnP_4 determined on a crystal by two-probe measurements along the needle axis (A) and perpendicular to the crystal axis (B), displayed as specific resistivity vs temperature and as Arrhenius plots, $-\ln(R) = f(1/T)$ with the respective linear regression fit (red line).

The conductivity along the *a* axis of the crystal is about 1 order of magnitude higher than perpendicular to the crystal axis. Displaying resistivity as Arrhenius plots, $-\ln(R) = f(1/T)$, linear correlations calculated for the perpendicular directions result in different slopes (Figure 4), indicating anisotropic behavior. The energies for the thermally activated electron transport are estimated to 0.11(5) eV along the axis and 0.21(5) eV in the perpendicular direction, giving γ-MnP_4 the character of a low-band gap semiconductor with anisotropic conductivity. It is possible that the intrinsic band gap is slightly higher due to the presence of impurity levels in the sample obtained by chemical transport with iodine. Because four-probe measurements are generally less biased by transition resistances of the contact wires, the four probe measurement was used to determine the specific conductivity. A room-temperature conductivity of 20 S/m was obtained (Figure S4). Examining the γ-MnP_4 DOS supports the diamagnetic, semiconducting behavior.

Controlling Polymorph Formation in MnP_4. The different modifications of MnP_4, including the new γ-MnP_4,

DOI: 10.1021/acs.inorgchem.5b01372
Inorg. Chem. 2015, 54, 8761−8768

are all stacking variants of two-dimensional layers built out of pentagons and hexagons of manganese and phosphorus. Because of the related crystal chemistry of these polymorphs it is difficult to predict which phase will result from a given synthesis. First-principles calculations are employed to predict the thermodynamics dictating phase formation.

First, the dynamic stability of the stacking variants was determined using phonon calculations via PHONOPY.[35] As observed in the phonon densities of states, Figure 5, all

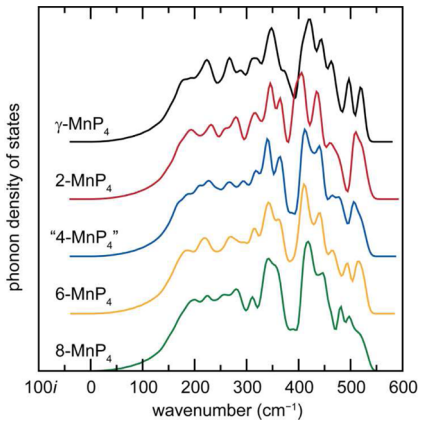

Figure 5. Phonon density of states of the stacking variants of MnP_4.

structures show similar shape with none producing imaginary vibrational modes; thus, they are all dynamically stable. An inspection of the eigenvectors at the Γ point of the first Brillouin zone reveals the lower modes (<200 cm^{-1}) are mainly vibrations in which the layers or packages of these shift parallel to each other. Interestingly, the interactions within the layers remain relatively rigid. Only at higher wave numbers, the rocking and stretching within the layers and perpendicular to the layers become prevalent. Similar characteristics are observed at all stacking variants, relatively independent of the stacking.

Thermodynamic potentials and properties can be derived from the phonon calculations.[39] Directly received from the phonon dispersion is the volume dependent Helmholtz energy (A). These values are calculated as the sum of the DFT-derived ground state energy (E_0) and the vibrational contributions from the phonon calculation. Because a large volume change is not expected between the phases as a function of temperature, the Helmholtz energy is a good approximation to the pressure dependent Gibbs Energy (G), which would require additional phonon calculations at different unit cell volumes. Plotting the Helmholtz energy as a function of temperature (Figure 6), the most energetically stable structure at low temperature is 6-MnP_4. Increasing temperature leads to a predicted structural transition at ≈800 K with the 2-MnP_4 structure becoming the lowest in energy. Thus, 2-MnP_4 is predicted to be the thermodynamically stable phase from approximately 800 K until 2000 K above which a second structural transition to 8-MnP_4 is predicted.

The successful synthesis of phase pure 2-MnP_4 using vapor transport highlights the formation of the thermodynamically most favorable structure in the midtemperature regime. To achieve the other polymorphs as phase-pure products, high-temperature routes combined with extended annealing at high temperatures should favor the formation of 8-MnP_4. On the other hand, the use of low-temperature routes should lead to the low-temperature phase 6-MnP_4. The new γ-MnP_4 phase

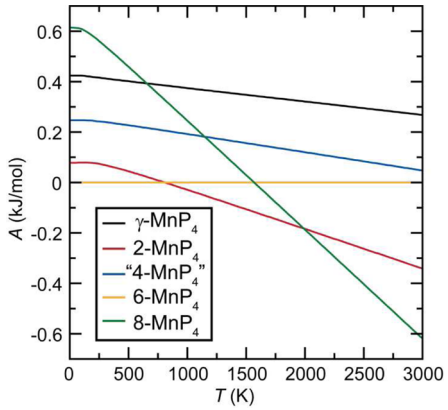

Figure 6. Helmholtz energy of the MnP_4 polymorphs as a function of temperature (relative to 6-MnP_4) from ab initio phonon calculations.

reported here is not predicted to be favorable at any temperature calculated and is likely a metastable phase. As a note, the energetic difference between all of the polymorphs is only ≈1 kJ/mol at 1000 K; this is equivalent to only 10 meV per formula unit. Because of the extremely small energy difference between the polymorphs, it will be difficult to dictate specific polymorph formation even with careful synthetic control.

Chemical Bonding from the Electronic Structures of MnP_4 Polymorphs. To understand the differences in chemical bonding that could aid the interpretation of the ab initio thermodynamic calculations, electronic structure calculations of all stacking variants were performed within the TB-LMTO method on structures that were optimized using VASP. The starting models for the VASP calculations were the experimentally determined structures (X-ray data).[7−9,12]

The density of states of γ-MnP_4 (Figure 7a) shows a band gap at the Fermi level, which is expected for the semiconducting material. Directly below the Fermi level, predominantly Mn 3d-states contribute to the DOS, and from −2 to −6 eV, mainly 3s and 3p states of P are present.

A bonding analysis was conducted on the basis of the crystal orbital Hamilton populations (COHP, see Figure 7b−d for γ-MnP_4) and their numerical integrals up to the Fermi level (ICOHP, see Table 3). The two different Mn−Mn bonding environments show unique bonding characteristics in accordance with their respective bond lengths. The COHP plot of the shorter Mn bond (2.91 Å) shows mostly bonding states below the Fermi level, while the unoccupied states above the Fermi level are antibonding. The longer Mn−Mn contact (3.74 Å) shows a negligible Hamilton population across the energy range examined based on the bond length in accordance with the very long bond length. Examining the P−P contacts in the structure indicate the next-neighbors within a layer range between 2.19 and 2.27 Å (average 2.24 Å), which is similar to the shortest covalent bond length in black phosphorus (2.22 Å).[40] Their average ICOHP value is −3.843 eV (32 bonds per unit cell, sum −122.98 eV per unit cell). These are the most-negative ICOHP values in the structure, indicating they provide most of the bonding character. The P−P distances between phosphorus atoms in different layers are generally larger and are not nearest-neighbor contacts. Their ICOHP values are mostly negligible, except for two contacts, which belong to the first coordination sphere. Their COHP-plots and distances are

DOI: 10.1021/acs.inorgchem.5b01372
Inorg. Chem. 2015, 54, 8761−8768

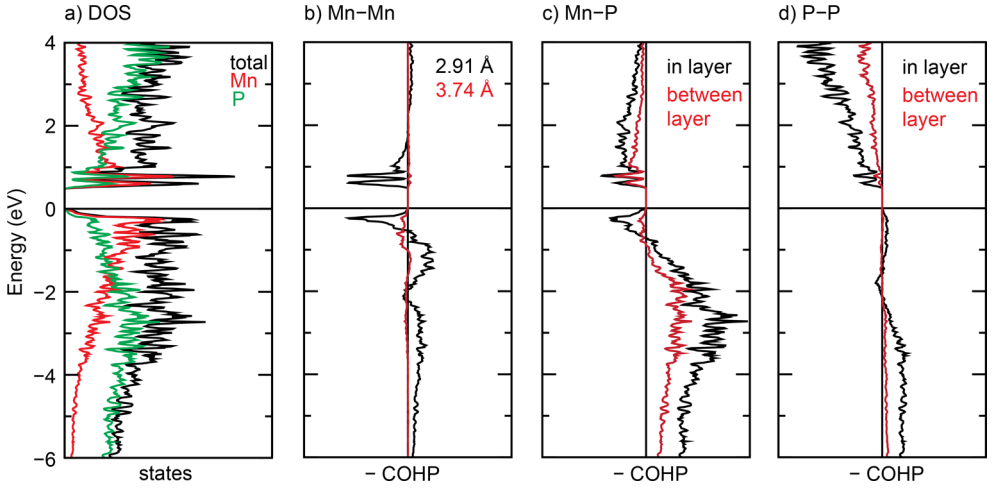

Figure 7. Density of states (DOS) and COHPs of various contacts in γ-MnP_4 calculated by TB-LMTO.

Table 3. ICOHP Values and Corresponding Distances (from VASP-Relaxed Structure) for Various Interatomic Interactions in γ-MnP_4

contact in γ-MnP_4	distance /Å (avg)	ICOHP/eV (per bond)	count	ICOHP/eV (per unit cell)
P−P (within layer)	2.19−2.27 (2.24)	−3.843	32	−122.98
P−P (between layers)	2.23−2.25 (2.24)	−3.624	8	−28.99
Mn−P (within layer)	2.21−2.33 (2.26)	−2.828	32	−90.49
Mn−P (between layers)	2.23−2.39 (2.30)	−2.608	16	−41.73
Mn−Mn (between layers)	2.91	−0.649	4	−2.59
Mn−Mn (between layers)	3.74	0.025	4	0.10

comparable to those in the layer, with a slightly smaller ICOHP value (ICOHP −3.62 eV at 2.24 Å).

From the perspective of the manganese atoms, they build distorted MnP_6 octahedral units, with one face capped by another Mn atom. In these polyhedra, the Mn−P contacts contribute the most to the integrated COHP curves. Their average ICOHP is −2.75 eV. The average Mn−P distance of 2.27 Å (48 bonds per unit cell) is similar to the sum of the atomic radii of Mn and P (2.27 Å).[41,42] The COHP plots of the Mn−P contacts show bonding character up to −0.8 eV below the Fermi level. In contrast, directly below the bandgap (0 eV to −0.8 eV), a region of antibonding contributions is found. For the Mn−P bonds, it is also possible to distinguish between those inside the layer and those between the layers, with those bonds inside the layer have larger ICOHP values than those between the layers (see Table 3).

This detailed bonding analysis indicates there is only a small difference between the average ICOHP values within the layers (See Table 3, for example P−P bond within layer −3.84 eV) and between the layers (P−P bond between layers −3.62 eV) for a single contact. However, when taking a summation over all ICOHPs within the unit cell, the findings show that the contribution of the intralayer interactions (−213.47 eV) surmount those of the interlayer interactions (−73.41 eV). Thus, describing the chemical bonding of these systems as layered stacking variants appears to not only be correct geometrically, but this finding is also supported by energetic considerations.

Expanding this electronic structure analysis to all of the MnP_4 variants supports the small free-energy differences between the polymorphs. Not only are all of the polymorphs semiconducting, but their density of states are nearly equal (see Figure 8). Conducting the same bonding analysis reveal that

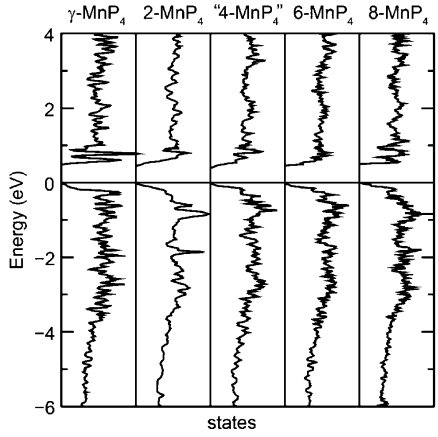

Figure 8. Density of states of known MnP_4 stacking variants calculated by TB-LMTO.

the orbital interactions also do not differ much between stacking variants as listed in Table 4. For example, the P−P bonds within the layer have averaged ICOHP values between −3.81 eV and −3.85 eV, with an arithmetic mean and a standard deviation of only −3.84(2) eV. In contrast, the ICOHP for the P−P bonds between the layers have an arithmetic mean and a standard deviation of −3.58(9) eV. Hence, the variance between the different stacking variants is much larger for the contacts between the layers than within the layer. The same can be observed for the Mn−P bonds (see, Table 4). This shows the stacking differences has only influence on the ICOHP values between the layers and even then only with minor changes. The bonding within the layers is nearly identical and is independent from the stacking.

DOI: 10.1021/acs.inorgchem.5b01372
Inorg. Chem. 2015, 54, 8761−8768

Table 4. ICOHP Values and Corresponding Distances (from VASP-Relaxed Structure) Comparing the Bonding Interactions in the Various MnP_4 Polymorphs

	2-MnP_4		4-MnP_4		6-MnP_4		8-MnP_4	
contact	distance /Å	ICOHP/eV	distance /Å	ICOHP/eV	distance /Å	ICOHP/eV	distance /Å	ICOHP/eV
P−P (in layer)	2.19−2.27	−3.85	2.19−2.27	−3.84	2.19−2.27	−3.85	2.19−2.30	−3.81
P−P (between layers)	2.27−2.28	−3.43	2.23−2.25	−3.61	2.23−2.27	−3.57	2.22−2.25	−3.66
Mn−P (in layer)	2.23−2.33	−2.84	2.21−2.32	−2.83	2.21−2.33	−2.83	2.21−2.38	−2.83
Mn−P (between layers)	2.23−2.34	−2.69	2.23−2.36	−2.62	2.22−2.36	−2.64	2.25−2.40	−2.66
Mn−Mn (short)	2.91	−0.65	2.91	−0.66	2.91−2.94	−0.64	2.92	−0.64
Mn−Mn (long)	3.73	0.03	3.72−3.75	0.03	3.73−3.75	0.03	3.76	0.03

Thus, from an analysis of the chemical bonding and electronic structures of these polymorphs it is clear the vibrational structure (thermodynamics) dictate the structure formation due to the similarity of the electronic structure.

CONCLUSIONS

This work reports the successful preparation and structure determination of a new manganese tetraphosphide stacking variant. The phase is named γ-MnP_4 due to the structural analogy with γ-FeP_4. Structure characterization was performed using crystalline powder and twinned single crystals, resulting in a description in space group *Cc*. Electrical and magnetic measurements show that the new modification of manganese tetraphosphide is semiconducting and diamagnetic. A theoretical investigation of all known stacking variants of MnP_4 shows that they are very similar in bonding, energy, and thermodynamic properties, which explains why the synthesis of these materials often lead to more than one of the stacking variants in the product. Based on electronic structure and phonon calculations, the 6-MnP_4 polymorph is thermodynamically favorable at lower temperatures, 2-MnP_4 is stable at intermediate temperatures, and high-temperature synthetic routes should favor the formation of 8-MnP_4. Following these free energy calculations, it appears the γ-MnP_4 crystal structure is most likely a metastable phase. Thus, it is not surprising that this structure remained unreported until now and even then could only be prepared using an iodine-assisted chemical transport method.

ASSOCIATED CONTENT

Supporting Information

The Supporting Information is available free of charge on the ACS Publications website at DOI: 10.1021/acs.inorgchem.5b01372.

Images and crystal facets of the γ-MnP_4 crystal used for electrical conductivity measurements, images of the experimental setup for the conductivity measurements, anisotropic displacements parameters from the single-crystal refinement, and the atomic positions and anisotropic displacement parameters from the structure refinement of γ-MnP_4 in space group *C*2/*c* (PDF)
Crystallographic data (CIF)

AUTHOR INFORMATION

Corresponding Authors

*E-mail: jbrgoch@uh.edu (J.Br.).
*E-mail: albert@ac.chemie.tu-darmstadt.de (B.A.).

Author Contributions

‖D.B.H. and M.H. contributed equally to this work.

Notes

The authors declare no competing financial interest.

ACKNOWLEDGMENTS

M.H. and J.Br. thank the Department of Chemistry and the Division of Research at the University of Houston for providing generous start-up funds. This work was also supported by the R. A. Welch Foundation through the TcSUH Robert A. Welch Professorship in High Temperature Superconducting (HTSg) and Chemical Materials (E-0001). The research presented here used the Maxwell/Opuntia Cluster(s) operated by the University of Houston Center of Advanced Computing and Data Systems (CACDS). D.B.H., C.L., and B.A. are grateful for the financial support of the BMBF programme INTEG.

REFERENCES

(1) Pöttgen, R.; Hönle, W.; von Schnering, H. G. In *Encyclopedia of Inorganic and Bioinorganic Chemistry*; John Wiley & Sons, Ltd: Hoboken, NJ, 2011.
(2) Von Schnering, H. G.; Hoenle, W. *Chem. Rev.* **1988**, *88*, 243−273.
(3) Shirotani, I.; Takaya, M.; Kaneko, I.; Sekine, C.; Yagi, T. *Solid State Commun.* **2000**, *116*, 683−686.
(4) Cheng, J. G.; Matsubayashi, K.; Wu, W.; Sun, J. P.; Lin, F. K.; Luo, J. L.; Uwatoko, Y. *Phys. Rev. Lett.* **2015**, *114*, 117001−117001.
(5) Tirado, J. L. *Mater. Sci. Eng., R* **2003**, *40*, 103−136.
(6) Souza, D. C. S.; Pralong, V.; Jacobson, A. J.; Nazar, L. F. *Science* **2002**, *296*, 2012−2015.
(7) Jeitschko, W.; Donohue, P. C. *Acta Crystallogr., Sect. B: Struct. Crystallogr. Cryst. Chem.* **1975**, *31*, 574−580.
(8) Jeitschko, W.; Rühl, R.; Krieger, U.; Heiden, C. *Mater. Res. Bull.* **1980**, *15*, 1755−1762.
(9) Rühl, R.; Jeitschko, W. *Acta Crystallogr., Sect. B: Struct. Crystallogr. Cryst. Chem.* **1981**, *37*, 39−44.
(10) Evain, M.; Brec, R.; Fiechter, S.; Tributsch, H. *J. Solid State Chem.* **1987**, *71*, 40−46.
(11) Fiechter, S.; Tributsch, H.; Evain, M.; Brec, R. *Mater. Res. Bull.* **1987**, *22*, 543−549.
(12) Paschke, D.; Wallinda, J.; Jeitschko, W. *J. Solid State Chem.* **1996**, *122*, 206−213.
(13) Jeitschko, W.; Donohue, P. C. *Acta Crystallogr., Sect. B: Struct. Crystallogr. Cryst. Chem.* **1972**, *28*, 1893−1898.
(14) Flörke, U.; Jeitschko, W. *J. Less-Common Met.* **1982**, *86*, 247−253.
(15) Braun, D. J.; Jeitschko, W. *Z. Anorg. Allg. Chem.* **1978**, *445*, 157−166.
(16) Rühl, R.; Jeitschko, W.; Schwochau, K. *J. Solid State Chem.* **1982**, *44*, 134−140.
(17) Jeitschko, W.; Rühl, R. *Acta Crystallogr., Sect. B: Struct. Crystallogr. Cryst. Chem.* **1979**, *35*, 1953−1958.
(18) Rubtsov, V. A.; Smolyarenko, E. M.; Trukkhan, V. M.; Yakimovich, V. N. *Cryst. Res. Technol.* **1986**, *21*, K93−K94.
(19) Dommann, A.; Marsh, R. E.; Hulliger, F. *J. Less-Common Met.* **1989**, *152*, 1−6.

DOI: 10.1021/acs.inorgchem.5b01372
Inorg. Chem. 2015, 54, 8761−8768

(20) Sheldrick, G. M. *Acta Crystallogr., Sect. A: Found. Crystallogr.* **2008**, *A64*, 112−122.
(21) Kresse, G.; Furthmüller, J. *Phys. Rev. B: Condens. Matter Mater. Phys.* **1996**, *54*, 11169−11186.
(22) Kresse, G.; Joubert, D. *Phys. Rev. B: Condens. Matter Mater. Phys.* **1999**, *59*, 1758−1774.
(23) Blöchl, P. E. *Phys. Rev. B: Condens. Matter Mater. Phys.* **1994**, *50*, 17953−17953.
(24) Perdew, J. P.; Burke, K.; Ernzerhof, M. *Phys. Rev. Lett.* **1996**, *77*, 3865−3868.
(25) Monkhorst, H. J.; Pack, J. D. *Phys. Rev. B: Condens. Matter* **1976**, *13*, 5188−5188.
(26) Andersen, O. K. *Phys. Rev. B: Condens. Matter* **1975**, *12*, 3060−3083.
(27) Skriver, H. L. *The LMTO Method*; Springer-Verlag, Berlin, 1984.
(28) Andersen, O. K.; Jepsen, O. *Phys. Rev. Lett.* **1984**, *53*, 2571−2574.
(29) Andersen, O. K.; Skriver, H. L.; Nohl, H.; Johansson, B. *Pure Appl. Chem.* **1980**, *52*, 93−118.
(30) Jepsen, O.; Andersen, O. K. *The STUTTGART TB-LMTO Program*; Max-Planck-Institut für Festkörperforschung: Stuttgart, Germany, 2000.
(31) Vosko, S. H.; Wilk, L.; Nusair, M. *Can. J. Phys.* **1980**, *58*, 1200−1211.
(32) Perdew, J.; Chevary, J.; Vosko, S.; Jackson, K.; Pederson, M.; Singh, D.; Fiolhais, C. *Phys. Rev. B: Condens. Matter Mater. Phys.* **1992**, *46*, 6671−6687.
(33) Blöchl, P. E.; Jepsen, O.; Andersen, O. K. *Phys. Rev. B: Condens. Matter Mater. Phys.* **1994**, *49*, 16223−16223.
(34) Dronskowski, R.; Bloechl, P. E. *J. Phys. Chem.* **1993**, *97*, 8617−8624.
(35) Togo, A.; Oba, F.; Tanaka, I. *Phys. Rev. B: Condens. Matter Mater. Phys.* **2008**, *78*, 134106−134106.
(36) Parlinski, K.; Li, Z. Q.; Kawazoe, Y. *Phys. Rev. Lett.* **1997**, *78*, 4063−4066.
(37) Knappschneider, A.; Litterscheid, C.; George, N. C.; Brgoch, J.; Wagner, N.; Beck, J.; Kurzman, J. a.; Seshadri, R.; Albert, B. *Angew. Chem., Int. Ed.* **2014**, *53*, 1684−1688.
(38) Knappschneider, A.; Litterscheid, C.; Brgoch, J.; George, N. C.; Henke, S.; Cheetham, A. K.; Hu, J. G.; Seshadri, R.; Albert, B. *Chem. - Eur. J.* **2015**, *21*, 8177−8181.
(39) Stoffel, R. P.; Wessel, C.; Lumey, M.-W.; Dronskowski, R. *Angew. Chem., Int. Ed.* **2010**, *49*, 5242−5266.
(40) Cartz, L.; Srinivasa, S. R.; Riedner, R. J..; Jorgensen, J. D..; Worlton, T. *J. Chem. Phys.* **1979**, *71*, 1718−1721.
(41) Pauling, L. *J. Am. Chem. Soc.* **1947**, *69*, 542−542.
(42) Pauling, L.; Kamb, B. *Proc. Natl. Acad. Sci. U. S. A.* **1986**, *83*, 3569−3571.

DOI: 10.1021/acs.inorgchem.5b01372
Inorg. Chem. 2015, 54, 8761−8768